Resolving taphonomic and preparation biases in silicified faunas through paired acid residues and X-ray microscopy

Gabriel S. Jacobs [1, 2], **Sarah M. Jacquet** [2], **Tara Selly** [2, 3], **James D. Schiffbauer** [2, 3], **John Warren Huntley** [Corresp. 2]

[1] Department of Geology, Cornell College, Mount Vernon, IA, USA

[2] Department of Geological Sciences, University of Missouri, Columbia, MO, United States

[3] X-ray Microanalysis Laboratory, University of Missouri, Columbia, MO, United States

Corresponding Author: John Warren Huntley
Email address: huntleyj@missouri.edu

Paired petrography and acid maceration has shown that preferential silicification of shelly faunas can bias recovery based on taxon and body size. Here, silicified fossils from the Upper Ordovician Edinburg Formation, Strasburg Junction, Virginia, USA, were analyzed using X-ray tomographic microscopy (µCT) in conjunction with recovered residues from acid maceration of the same materials to further examine sources of potential bias. Results reveal that very small (< ~1 mm) fossils are poorly resolved in µCT when scanning at lower resolutions (~30µm), underestimating abundance of taxa including ostracods and bryozoans. Acid maceration, meanwhile, fails to recover poorly silicified fossils prone to disarticulation and/or fragmentation during digestion. Tests for patterns of breakage, however, indicate no significant size or taxonomic bias during extraction. Comparisons of 3-D fossil renders and extracted residues of individual fossils reveal taxon-specific patterns of fragmentation and allow biostratinomic and preparational breakage to be differentiated. Paleoecological ordinations and cluster analyses of datasets based on µCT data and residues produce generally concordant results but indicate that true variation between taxonomic composition of our samples is compromised by the resolvability of small size classes in µCT imaging, limiting the utility of this method for addressing paleoecological questions in these specific samples. We suggest that comparability of results will depend strongly on the sample size, taphonomic history, textural, and compositional characteristics of the samples in question, as well as µCT scan parameters; applying similar methods to different deposits will help to generalize conclusions drawn on the relative strengths and weaknesses of the methods.

Resolving taphonomic and preparation biases in silicified faunas through paired acid residues and X-ray microscopy

Gabriel S. Jacobs[1,2], Sarah M. Jacquet[1], Tara Selly[1,3], James D. Schiffbauer[1,3], John Warren Huntley[1]

[1] Department of Geological Sciences, University of Missouri, Columbia, MO, USA

[2] Department of Geology, Cornell College, Mount Vernon, IA, USA

[3] X-ray Microanalysis Laboratory, University of Missouri, Columbia, MO, USA

Corresponding Author:

John Warren Huntley[1]

101 Geological Sciences Building, University of Missouri, Columbia, MO 65211, USA

Email address: huntleyj@missouri.edu

Abstract

Paired petrography and acid maceration has shown that preferential silicification of shelly faunas can bias recovery based on taxon and body size. Here, silicified fossils from the Upper Ordovician Edinburg Formation, Strasburg Junction, Virginia, USA, were analyzed using X-ray tomographic microscopy (μCT) in conjunction with recovered residues from acid maceration of the same materials to further examine sources of potential bias. Results reveal that very small (< ~1 mm) fossils are poorly resolved in μCT when scanning at lower resolutions (~30μm), underestimating abundance of taxa including ostracods and bryozoans. Acid maceration, meanwhile, fails to recover poorly silicified fossils prone to disarticulation and/or fragmentation during digestion. Tests for patterns of breakage, however, indicate no significant size or taxonomic bias during extraction. Comparisons of 3-D fossil renders and extracted residues of individual fossils reveal taxon-specific patterns of fragmentation and allow biostratinomic and preparational breakage to be differentiated. Paleoecological ordinations and cluster analyses of datasets based on μCT data and residues produce generally concordant results but indicate that true variation between taxonomic composition of our samples is compromised by the resolvability of small size classes in μCT imaging, limiting the utility of this method for addressing paleoecological questions in these specific samples. We suggest that comparability of results will depend strongly on the sample size, taphonomic history, textural, and compositional characteristics of the samples in question, as well as μCT scan parameters; applying similar methods to different deposits will help to generalize conclusions drawn on the relative strengths and weaknesses of the methods.

Introduction

Silicification is a common preservational mode in the fossil record, especially in the early Paleozoic (Butts, 2007; Butts & Briggs, 2010), involving the fabric-specific replacement of calcareous biota (calcite and aragonite) with silica, typically as chalcedony, opal, or sometimes as sparry quartz cement. While the fine-scale mechanisms of silicification in limestone remain unclear, the overall process is simple: pore fluids containing dissolved silica (whether volcanic, hydrothermal, or biogenic in origin) undergo transport and react with the host rock, causing contemporaneous dissolution of calcite and/or aragonite and the precipitation of silica through mechanisms involving both pH change and pressure dissolution (Maliva & Siever, 1988).

Due to their enhanced resistance to other fabric-destructive diagenetic process (Schubert, Kidder & Erwin, 1997), silicified fossils are typically preserved in great fidelity and abundance. Moreover, the replacement process frequently replicates fine morphological details if not internal microstructure, and the insolubility of silica to dissolution by acid allows such material to be prepared chemically rather than mechanically (Baars, 2008; Butts, 2014). Acid maceration is a broadly employed technique used to extract silicified fossils from limestone, relying on the high solubility of calcite in acidic solution and the comparatively low resistance of micritic matrix to alteration or dissolution (Donald W. St. Clair, 1935; Grant, 1989). However, such extraction methods can introduce potential biases that might skew perceptions of paleoecological studies investigating silicified specimens (Pruss, Payne & Westacott, 2015). Two primary sources of bias that can readily be identified include the differential likelihood that a given specimen will (1) silicify during diagenesis, and (2) once silicified, survive preparation and be recovered.

If biases in differential preservation and recovery methods go unaccounted for, certain types of analyses can be more severely affected. Systematic descriptions of organisms may be only mildly affected by the underrepresentation of some ontogenetic stages relative to others, but studies specific to the paleoecology or biofacies of an assemblage can suffer in quality due to their reliance on an accurate assessment of which biota are present in the deposit. For example, the near absence of a guild of predators or the preferential breakage of certain types of shell ornamentation might drastically alter the interpretation of trophic relationships and biotic interactions. Similarly, the loss of fossils in a certain size range during preparation can affect interpretations of biostratinomic processes. Because these biases may skew paleoecological interpretations of fossil assemblages, quantifying or at least constraining them can improve confidence in the results of research relying on this common preparatory method.

Previous research has attempted to account for preservational and preparation bias in acid maceration of silicified fossils. Pruss et al. (2015)compared the relative abundances of fossil taxa in 11 hand samples of the Triassic Virgin Limestone Member of the Moenkopi Formation, from which the authors made a petrographic thin section and extracted fossil specimens via buffered acetic acid maceration. In general, echinoderms and gastropods were disproportionally over-represented in residues while bivalves were more likely to be identified in thin-section point counts (Pruss, Payne & Westacott, 2015).

Two questions not addressed by the aforementioned study are those of body size bias and breakage patterns. Since petrographic analysis can identify fossils by their

taxonomic group but offers minimal useful information with respect to their dimensions, detecting differences in body size distribution between thin section grains and fossils recovered in residues is not feasible. Similarly, it is impossible to tell by extraction methods whether fossils in residues suffered damage during digestion and washing or whether the breakage occurred prior to burial. Because thin sections and residues do not record the same fossils but rather disjoint subsets of the total fossils within the hand sample, no true pre and post comparison can be made. Indeed, since both methods applied in the Pruss et al. (Pruss, Payne & Westacott, 2015) study are destructive, a single fossil cannot be recorded by both. This inherent limitation can be avoided, however, by pairing a non-destructive whole-rock analytical method with acid maceration. X-ray tomographic microscopy (μCT) is well-suited to such an approach, allowing compositional and textural differences within a sample to be imaged as a grayscale representation of density variation in three dimensions, revealing fossil material within. By then subjecting the sample to acid maceration, individual fossils can be resolved and measured before and after chemical preparation, and any breakage or loss documented and quantified.

Herein, we employ a paired approach combining μCT-generated three-dimensional volume data of bulk rock samples with investigation of subsequently acid-extracted insoluble residues from the same scanned samples test the hypothesis that smaller fossils would be disproportionately less likely to survive preparation and be recovered from acid-digested residues and to further assess and quantify introduced biases and their implications for paleoecological studies. For this study, we used prepared cores of carbonate bulk rock samples from the Edinburg Formation of Virginia,

USA, which is well-known to host abundant and diverse silicified Ordovician marine fossils (Whittington & Evitt, 1953; KRAFT, 1962). The pervasive silicification of the fossils within this unit makes it amenable to delivering sufficient contrast between the skeletal material and the host matrix using μCT.

Materials & Methods

Geological Setting

The Edinburg Formation is an Upper Ordovician unit of massively bedded black limestone with occasional shaley interbeds, representing deep ramp to basinal deposition at the northwest of the Taconic foreland basin system after drowning of shallower ramp carbonate facies including the underlying Lincolnshire Limestone (Holland & Patzkowsky, 1996). Potassium bentonites derived from Taconic volcanism are sporadically present in the sediments of the foreland basin and have been sampled for radiometric ages, most notably the Millbrig bed, which lies up section of the Edinburg in the Martinsburg Formation and has a U-Pb date of 452.86 Ma (Mitchell et al., 2004; Sell, Ainsaar & Leslie, 2013).

All samples in this study were collected from the Liberty Hall facies of the Edinburg Formation exposed at Strasburg Junction rail cut, a well-studied site in the Shenandoah Valley of Virginia (Fig. 1, Table 1; (Cooper & Cooper, 1946; Whittington & Evitt, 1953; Read, 1980; Jacobs & Carlucci, 2019). Hand sample observations revealed two starkly different lithologies (Table 1). Rocks from Horizon 1, approximately 0.5 m above the contact between the Lincolnshire Limestone and Edinburg Formation, were coarse-grained, with a sparry or dismicritic texture likely indicative of recrystallization during early diagenesis. Sparse fossils and possible intraclasts visible on fresh surfaces were weakly aligned

171 with the direction of original bedding, suggesting directional sorting during deposition.
172 Horizons 3, 4, 5, and 6 cropped out over 30 m up section (Table 1) and were finely
173 grained with only occasional sparry or hematitic grains. Fossils, where visible on fresh
174 or weathered surfaces, were oriented randomly to original bedding and comprised
175 arthropods, brachiopods, and occasional crinoid ossicles. Rocks from these horizons
176 also displayed heavy rinds on weathered surfaces, frequently stained rusty orange to
177 pale yellow with iron oxides/oxyhydroxides.

178 **Fossil Extraction**

179 From the five horizons with fossils visible on weathered surfaces, 15 samples were
180 prepared as cylindrical cores (Table 1), approximately 2 cm in diameter and ranging
181 from 1 to 4 cm in height, normal to bedding. Each core was imaged via X-ray
182 tomographic microscopy using a Zeiss Xradia 510 Versa X-ray microscope with an
183 isotropic voxel size of approximately 30 μm, producing three-dimensional renders of the
184 core interiors. All μCT scans were processed using Dragonfly software Build 941–
185 v.4.2.2 for Windows, Object Research Systems (ORS) Inc, Montreal, Canada, 2018
186 (http://www.theobjects.com/dragonfly). Post-image processing within the software was
187 conducted to reduce imaging artifacts using the Ring Removal and Median filters.
188 Regions of high brightness (corresponding to high-density ferrous material) and low
189 brightness (corresponding to low-density siliceous material) relative to the local
190 background were thresholded and manually segmented, excluding regions at the very
191 top and bottom of cores due to persistent boundary artifacts. Due to radial and
192 longitudinal variation in background brightness across the cores, multiple brightness
193 thresholds were used to segment siliceous material in some cores; in such cases, the

194 total siliceous volume is the union of the volumes from segmentation by the various
195 thresholds. Segmented volumes for ferrous and siliceous material were refined by
196 removing small (<100 voxel total volume) islands and were then partitioned into distinct
197 regions-of-interest (ROIs), using 6-connectivity (voxels considered to be connected if
198 sharing faces rather than only edges or vertices) for both purposes. Individual fossils
199 and other objects were identified among these ROIs by visual inspection in 3-D
200 representations of voxels and against individual 2-D projections of μCT imagery. In
201 cases where a fragmentary or incompletely resolved fossil fell into multiple non-
202 connected ROIs, those ROIs were merged into one; in cases where a single ROI
203 contained multiple contiguous objects, it was manually partitioned.

204 After each core had been imaged with μCT, they were macerated in 10% acetic
205 acid to dissolve calcareous material until fully disaggregated and no longer visibly
206 evolving gas bubbles. Insoluble residues were washed with water and sonicated in 30-
207 second intervals, iterating until the supernatant ran clear. This washing process was
208 then repeated using Calgon solution (0.052 M $Na_6(PO_3)_6$, 0.286 M $NaHCO_3$) as a
209 deflocculant, sonicating as before, until all loose clay was removed. Cleaned residues
210 were then washed over a 250-μm sieve, oven dried, and picked for identifiable fossils.

211 **Statistical Analyses**

212 Following scanning and segmentation, each object resolved in the μCT data was
213 measured for minimum, maximum, and mean three-dimensional Feret diameter. Fossils
214 that could be confidently identified to at least the phylum level were scored for additional
215 taxon-specific features and anatomical measurements (Table 2).

Fossils recovered from residues were photographed using a GIGAmacro Magnify2 Robotic Imaging System with Canon EOS Rebel T8i DSLR and Nikon T1 1× and 3× objectives. For large specimens, additional photographs were taken under a reflected light microscope (Nikon SMZ1500 tethered to a Nikon D600 DSLR) to record features not visible in top-down view. Photographs were processed and analyzed with FIJI/ImageJ software, using the Trainable Weka Segmentation plugin to isolate fossils against the image background (Andreola et al., 2004a,b; Schindelin et al., 2012). Each fossil was measured for minimum and maximum two-dimensional Feret diameter as well as taxon-specific measurements corresponding to those taken from µCT data (Table 2).

For each core, both the segmented µCT render and acid residues were counted for the total abundance of fossil taxa. Trilobites were identified to the family level based on their general geometry, furrow pattern, and, in residues, their prosopon. Trilobite material not reliably assignable to a single family was treated as a separate category. Prosopon and other textural features were not easily resolvable in the µCT dataset, and so were not generally considered for taxonomic assignment in counts based on µCT results. Bryozoans were classified by growth form either as thin-branching, thick-branching, or fenestrate. Ostracods, gastropods, and bivalves were not further classified due their generally small sample size and coarse silicification, precluding the reliable identification of taxonomically relevant features.

Using R statistical software, datasets were subjected to NMDS in three dimensions based on the Bray-Curtis dissimilarity index, using the *metaMDS* function provided in the *vegan* package (Dixon, 2003; R Core Team, 2021). Sites with no

239 counted fossils were excluded from the analysis. Further paleoecological analysis of
240 taxon abundances within and between samples was performed using PAST statistical
241 software, calculating ecological dominance within samples (Simpson's *D*) and
242 assessing compositional similarity between samples using the Bray-Curtis index (Hammer
243 & Harper, 2001, 2022).

244

245 ## Results

246 A total of 582 objects were resolved via µCT, 460 as a low-opacity siliceous phase and
247 122 as a high-opacity ferrous phase; of these, 241 siliceous objects and 14 ferrous
248 objects were identifiable to at least a coarse taxonomic level, with the remaining 219
249 and 108 respectively left unidentified (Fig. 2). Siliceous fossils were dominated by
250 trilobites (n = 225), of which slightly less than half (n = 99) could be confidently assigned
251 to a family classification; including Asaphidae (c.f. *Isotelus*), Cheiruridae (*Ceraurus*),
252 Metagnostidae (*Trinodus*), Pterygometopidae (*Calyptaulax*), Raphiophoridae (*Ampyx*,
253 *Lonchodomas*), and Remopleurididae (*Remopleurides*), all of which are previously
254 known from this site (Whittington & Evitt, 1953; Evitt, 1961). Non-trilobite siliceous material
255 consisted of thin-branching and fenestrate bryozoans and a single valve from an
256 ostracod. Ferrous fossils were mostly gastropods, with two bivalves, one possible thin-
257 branching bryozoan, and one infilling of a raphiophorid cranidium (Table 3). This
258 cranidium was counted towards siliceous and ferrous µCT object totals due to being
259 preserved as silicified cuticle filled in by moldic pyrite but was counted as one individual
260 in taxon totals (Fig. 2D).

261 Residues yielded 1,349 recognizable objects, 1,222 preserved as silica, 125 as
262 iron minerals (pyrite, hematite, and/or limonite), and the remaining two as other

materials (one of them appears to be a crystal of muscovite; neither was identifiable as a fossil). Nearly all siliceous fossils were identifiable to at least a coarse taxonomic level, with only 48 left unidentified. Conversely, 113 of the iron-preserved objects could not be identified. Siliceous objects in residue were made up largely of trilobites, fragments of thin-branching bryozoans, and ostracods. All trilobite genera represented in µCT were found also in residues, along with trilobites from the family Odontopleuridae (c.f. *Ceratocephala*). The remainder consisted of thick-branching and fenestrate bryozoans along with occasional brachiopod fragments. Ferrous fossils were exclusively represented by gastropods, with the exception of a single bivalve (Table 3).

Tests of Preparation Bias

A contingency table was constructed containing µCT identified specimens counts, broken down by taxonomic grouping and by presence or absence in residues. The relationship between taxon and recovery was investigated using Pearson's χ^2 test (Table 4). The only taxonomic group which deviated significantly ($p < 0.05$) from overall likelihood of recovery was Unidentified Trilobita, material clearly from trilobites but lacking anatomical features in µCT sufficient to assign it to a family; such fossils identified in µCT are disproportionately unlikely to be recovered in residues.

Application of Pearson's χ^2 test to total counts of taxa identified in µCT and in residue found strong support ($p < 0.000001$) for different proportional abundances in the two preparation types (Table 5). Raphiophorids, remopleuridids, unidentified trilobites, bivalves, and gastropods are significantly ($p < 0.05$) more abundant in µCT, while branching bryozoans (thin and thick) and ostracods are significantly more abundant in residues.

The presence of size bias in the likelihood of recovery was evaluated using the Mann-Whitney U-test with a null hypothesis of no difference in medians and a standard threshold of significance of $\alpha = 0.05$ (Mann & Whitney, 1947). In comparisons between fossils identified in both µCT and residue and those identified in µCT but *not* in residue, there was no statistically significant difference of maximum ($p = 0.544$), minimum ($p = 0.088$), or mean ($p = 0.244$) Feret diameters, nor of elongation factor ($p = 0.159$) defined as the ratio of maximum to minimum Feret diameters. However, when testing overall distributions of size between all fossils identified in µCT and all those found in residue, the U-test found a dramatic difference in maximum Feret diameter ($p = 1.75 \times 10^{-79}$) between the medians of the two groups.

Exploratory Paleoecological Ordinations

NMDS performed separately on the µCT (Table 6) and residue (Table 7) datasets resulted in ordinations with stress scores of 0.06 and 0.08, respectively (Fig. 4). Taxon loadings in both ordinations consistently grouped bivalves and gastropods nearby each other, which may reflect either a shared infaunal environment or instead early burial conditions conducive to pyritization in those deposits. However, the low abundance of bivalves (2 in µCT, 1 recovered from residues, always alongside multiple gastropods) makes this apparent association tenuous. It is noteworthy that disseminated pyritization in the form of non-fossil granules was present in several samples (e.g., 05-C4) that contained no mollusks, suggesting that the presence or absence of mollusks in a sample may reflect their abundance in the paleoenvironment and is not solely controlled by whether early burial chemistry allowed pyritization to proceed.

Ordinations of both µCT and residues tended to group medium-sized benthic trilobites (raphiophorids, pterygometopids, and cheirurids) together along with unidentified trilobite material (most of which likely derived from one of those families), with pelagic trilobites (remopleuridids) plotting closer to gastropods and bivalves. Asaphids, likely represented here by the extremely large benthic trilobite *Isotelus*, consistently fall near the latter cluster but are represented only by fragments of cuticle. The ordination position of agnostids, whose life habit remains controversial (Fortey & Owens, 1999), is inconsistent between µCT and residues, falling near the benthic and pelagic trilobite clusters in those analyses, respectively. In both cases, they are closely accompanied by ostracods (which can occupy pelagic or benthic niches and whose life habit was not interpreted in this study). Due to the extreme disparity between identification in µCT and recovery in residues of ostracods, their location within the ordination for µCT data is likely not informative.

Thin-branching and fenestrate bryozoans plotted relatively close together, forming an isolated cluster. Thick-branching bryozoans were not closely associated with the other two morphotypes in the residue ordination and were not detected in µCT.

Samples from individual horizons tended to fall near each other in loose association. Two main clusters are apparent in both residue and µCT ordinations: one characterized by low NMDS1 scores and dominated by bryozoans, and one with higher NMDS1 scores and dominated by arthropods (trilobites and ostracods).

For each sample, dominance was computed for both µCT (Table 6) and residue (Table 7) taxon totals, with 95% confidence intervals based on 9999 bootstrap replicates (Fig. 5). The results of this analysis differed notably between the two; µCT dominance values

fell in a tight band between 0.25 and 0.40 (excepting two outliers with n<3), while residue dominance values had a bimodal distribution with one group of values between 0.40 and 0.65 and another falling between 0.15 and 0.30. (Fig. 5) Rarefaction curves were calculated for both μCT (Table 6) and residue (Table 7) counts of each sample using PAST (Hammer & Harper, 2022; Fig. 6). Curves were visually inspected for the presence of an inflection point as a rough qualitative assessment of sampling completeness; a sample's curve "leveling off" (sudden decrease in slope) is considered informal evidence that taxa in the true population are well-represented in the sample (Raup, 1975; Sanders, 1968). This inflection point was observed in residue counts from most samples (prominently in 03-C1, 03-C3, 04-C1, and 06-C3), but not in μCT counts. This suggests that the smaller total counts of individuals in μCT data are leading to the non-recovery of rarer taxa. Such under-sampling is a liability of ecological analyses based on those samples.

Cluster Analysis

Multivariate cluster analyses were performed in PAST to provide alternate metrics of similarity in the paleoecological composition of the samples, using the Bray-Curtis index as before (Bray & Curtis, 1957; Hammer & Harper, 2022). Dendrograms with branch length scaled to similarity were constructed for μCT counts, residue counts, and a combined dataset treating μCT and residue counts for each sample as two separate sites. (Figs. 7 and 8) Cluster analysis of μCT counts grouped samples from Horizon 04, and treated Horizon 05 similarly, but scattered samples from Horizons 03 and 06 across the tree. Using residue data, Horizon 05 formed a cluster as before but Horizon 04 split, with cores 04-C2 and 04-C3 remaining close but 04-C1 further

355 removed; Horizons 03 and 06 were dispersed as in the µCT tree. In both trees, samples
356 from Horizon 01 were far removed from other samples, tending to form a cluster basal
357 to the rest of the samples.

358 The combined tree retains the general close groupings of the two individual trees
359 due to sharing the same dissimilarity metric (Fig. 8). Notably, even for Horizons (01, 04,
360 05) whose samples tended to cluster in both the µCT and residue trees, those clusters
361 are not closely related in the overall analysis; there are few clear patterns in this tree,
362 but µCT samples tend to cluster more closely with other µCT samples, and residue
363 samples with residue samples, than do µCT and residue counts of the same sample or
364 even of samples from the same horizon.

365

366 ## Discussion

367 ### Size and Taxon Effects on Recovery

368 We hypothesized at the outset of this study that body size would be negatively
369 associated with likelihood of recovery in residues; larger fossils may be more
370 susceptible to breakage, and larger organisms with thicker skeletal elements may not
371 fully silicify, producing a brittle outer husk. However, the results of our analysis do not
372 support this possible effect. While fossils recovered in residue have a smaller median
373 body size than those resolved in µCT, this appears to be due not to preferential
374 breakage of larger fossils during washing but rather disproportionate non-resolution of
375 smaller fossils in µCT datasets. Rather than µCT acting as a baseline to test the biases
376 of acid maceration based on body size, the results of this study suggest the opposite.

377 Revealing that the number of unidentified trilobite fossils recognized in µCT is
378 significantly less likely to be recovered in residue is to be expected. Fragmentation and

379 incomplete preservation are common causes for trilobite material to lack identifying
380 characteristics, and both are likely to promote further breakage and degradation during
381 washing by compromising the structural integrity of the sclerite. This may also influence
382 likelihood of recovery by impeding identification of the fossil in residue; a fragment of
383 cuticle lacking identifying characteristics is less likely to be recognized as corresponding
384 to an object observed in μCT, and minor breakage is likely to disrupt recognizable
385 aspects of its outline and other key features.
386 Overrepresentation with respect to the abundance of pyritized taxa (gastropods
387 and bivalves) in μCT may be the result of the high contrast between iron-bearing
388 phases and the matrix, making such fossils easier to resolve in μCT than otherwise-
389 comparable siliceous fossils. Alternatively, this may represent preferential breakage of
390 pyritized material during washing due to differences in replacement texture. Ostracods,
391 meanwhile, are disproportionately overrepresented in residue due to their small size
392 making them difficult to resolve in μCT at the resolution used in this study. Branching
393 bryozoans similarly also suffer from this, but their numbers in residue are likely inflated
394 by fragmentation of large individuals into many smaller ones.
395
396 **Nonrecovery Bias**
397 Diagenetic bias arises from a variety of sources and is heavily dependent on shell
398 microstructure, organic matter, and availability of reactive and replacive ions to the
399 shell. It is well-documented that certain taxa are more susceptible to silicification than
400 others, and even within taxa textural differences can make certain skeletal elements
401 more likely to be preserved than others (Roberta L. Daley (*), 1996; Cherns et al., 2011;

Butts, 2014). Organic matter content within a shell also influences the likelihood of silicification by providing nucleation sites for the deposition of silica, though the chemistry of this is complex (Wallace, DeYoreo & Dove, 2009; Butts, 2014). Similarly, replacement via pyrite tends to initiate at sites of organic matrix in the shell but is also dependent upon reducing microenvironments and/or microbial zonation within the sediment (FISHER, 1986; Canfield & Raiswell, 1991; Schiffbauer et al., 2014).

Further biases can arise from the sample extraction and preparation process itself. During washing, larger fossils may be tumbled against other grains or container walls, leading to abrasion or breakage, while smaller fossils may be crushed beneath larger objects as grains settle. Elongated grains may be more prone to breakage than spheroidal grains of the same volume due to a lower minimum cross-sectional area, which can lead to taxon or sclerite bias against fossils with rod-like geometry, such as branching bryozoans and the spines of some trilobites. Breakage during preparation can cause taxa to be undercounted due to indiscriminate destruction of individuals or damage sufficient to remove recognizable features. Paradoxically, it can also inflate taxon counts by turning one fossil into many still-recognizable fragments. These overlapping effects can produce a wide variety of biases in size and shape, and the cumulative effect on measurements of abundance cannot reasonably be predicted *a priori*.

Composition of the host rock can further impose preparation-related biases. For instance, well-cemented rocks frequently require longer maceration periods than poorly consolidated ones, while argillaceous rocks may need more thorough washing to drive off insoluble clays, often including sonication. The longer sediment is washed and

manipulated, the more breakage tends to occur, making matrix texture an important factor of preparation bias. While the acid maceration processes can be accelerated by using alternative acids, such as hydrochloric, the violent effervescence caused by the intensity of the reaction can also have a deleterious effect on the extraction of delicate forms.

Artifacts and Limitations of µCT

While a powerful tool for visualization, µCT does present some unavoidable sources of potential error: artifacts arising from specimen capture and processing, particularly the “hardening” of the X-ray beam through preferential absorption of lower-energy photons by the sample. Beam hardening is a ubiquitous issue in µCT, but not all hardening artifacts are of equal impact. Since the beam is slightly hardened by passing through the outer surface of the sample, the interior is always slightly darkened relative to the outermost layer; these “cupping artifacts” are produced predictably based on sample geometry and can be corrected relatively easily (Schladitz, 2011; Jung et al., 2011; Abel, Laurini & Richter, 2012).

Heterogeneous samples suffer from more vexing artifacts. Regions of higher-density material (e.g., iron minerals in sediments, bones in biological samples) can drastically harden beams passing through them, causing dark blotches to appear around bright features within a sample and especially in the spaces between multiple bright features. These artifacts are far more difficult to correct due to their irregular shape and remain the subject of ongoing research in economic geology and other materials science fields (Remeysen & Swennen, 2006; Park, Chung & Seo, 2015; Bam et al., 2019). Given the abundant pyrite in the material examined in this study, this stands as a caveat to the

448 results reported here; similar methods applied to rocks with lower density variation may
449 yield clearer μCT data and therefore more complete identification of fossils within the
450 samples. Filtering during pre-processing, or correction applications in post-processing
451 software packages, can reliably improve these artifacts, but often at the cost of
452 introducing noise along the axis of sample rotation (Kyriakou, Prell & Kalender, 2009; Yousuf &
453 Asaduzzaman, 2009).

454 The 3-D nature of μCT data can lead to more conceptual issues when drawing
455 comparisons to features in corresponding 2-D imagery. One such caveat relates to
456 resolution, the smallest possible distance between features that can be resolved by an
457 imaging method. Not only is this distance always larger (coarser) than the side length of
458 pixels or voxels making up the image produced, but it depends on the nature of the
459 sample, with more internally complex and heterogeneous materials having larger
460 effective resolution than homogeneous ones (Elkhoury, Shankar & Ramakrishnan, 2019).
461 Resolution can also be larger and more challenging to measure in 3-D imaging than in
462 2-D. Determining by observation whether adjacent features are connected or distinct in
463 a 2-D plane is relatively easy, but due to limitations of how displays and human vision
464 project three dimensions down to two, the equivalent task in 3-D volume is more
465 challenging. In practice, this means that features near the theoretical resolution limit of
466 3-D imaging methods are likely to be lost, especially when interpreted by human
467 observers. When assessing body size effects on recovery in 3-D μCT imagery versus 2-
468 D residue photographs, this disparity in effective resolution should be taken into
469 account.

470 **Relevance for Paleoecological Interpretation**

Broad categories of biofacies are generally consistent between residue- and µCT-derived taxon abundances as interpreted using NMDS. While total counts for µCT are much lower than those of residues, relative abundances in the former largely recapitulate the latter with some notable exceptions; ostracods are almost absent from µCT data, due to resolution constraints imposed from the diameter of the cores, even when highly abundant in residues, and bryozoan counts tend to be much higher in residues than in µCT due to breakage transforming one large fragment into many small fragments. For this reason, the application of µCT data alone to describe paleoecological structure should be undertaken with caution. Ordinations used in paleoecology are sufficiently complex that such biases in recovery can, by introducing error and uncertainty upstream, irreparably taint conclusions drawn downstream.

Overall, the use of µCT counts on their own to characterize silicified remains in these limestone biofacies is of uncertain value. Sample volume constraints make bulk samples unfeasible, and the cost of instrument time can be a roadblock to replication and large-scale sampling. However, µCT may be best suited when chemical preparation is dangerous or impractical due to matrix or fossil mineralogy, or when studying sponges, bryozoans, corals, or other modular organisms for which fragmentation during washing can obscure or inflate the number of individuals present. Samples best suited to the approach outlined in this study will be densely fossiliferous (mitigating the limitation of sample volume), bear taxa with morphological features conducive to identification in µCT (related to shape rather than texture) and contain grains more susceptible to dissolution than the matrix or cement joining them together. Such rocks should also have a strong contrast in density (and therefore X-ray attenuation) between

grains and matrix, but with relatively little influence of beam hardening artifacts. Conodonts and other phosphatic fossils, for example, are occasionally known from silicified sediments, and characterizing taxonomic assemblages using μCT techniques may constitute a welcome alternative to digestion with the notoriously toxic and hazardous hydrofluoric acid normally used to liberate fossils from siliceous cements (Green, 2001).

Conclusions

The main goal of this study was to quantify the effects of taxonomic affinity and body size on the likelihood of fossil recovery, but it is the qualitative results that may have the broadest relevance to further work. Breakage remains an unavoidable concern with acid maceration, but the degree to which breakage rates depend on body size and taxonomic factors likely varies substantially between deposits. This variation can stem not only from easily observable sedimentological features such as grain size and composition but also from redox chemistry and solute profiles of pore fluids during burial and early diagenesis, which can be challenging to infer from samples without more in-depth geochemical analyses. Original shell composition, both in terms of organic content and aragonitic versus calcitic (high- or low-magnesium) mineralogy is likely relevant due to its influence on the spontaneity and kinetics of silicification chemistry. Information on the breadth of variation is limited but suggests a wide range of possible taxonomic outcomes based on sample lithology.

While μCT imaging of silicified fossils in limestone matrix can resolve morphological features of interest, the issues faced in this specific study may limit this technique's ability to answer broader paleoecological questions. Analyzing original rock contents as

a means of detecting breakage during preparation may be valuable as a control on fragmentary abundance counts, but limitations of sample size and the potential for taxonomic bias to affect ordinations present serious pitfalls to analysis or characterization of biofacies. It can, however, be useful in establishing broad categories if not finer gradations between related assemblages. Since the drawbacks resulting from beam hardening and other µCT artifacts are heavily dependent on the properties of the sample, these methods may prove more effective when applied to rocks containing different fossil taxa or with different lithologic compositions from the materials studied here.

Acknowledgements

We gratefully acknowledge L.G. Huntley for assistance with fieldwork and reviewers A, B, and C for constructive comments.

References

Abel R, Laurini C, Richter M. 2012. A palaeobiologist's guide to "virtual" micro-CT preparation. *Palaeontologia Electronica*. DOI: 10.26879/284.

Andreola F, Castellini E, Manfredini T, Romagnoli M. 2004a. The role of sodium hexametaphosphate in the dissolution process of kaolinite and kaolin. *Journal of the European Ceramic Society* 24:2113–2124. DOI: 10.1016/S0955-2219(03)00366-2.

Andreola F, Castellini E, Manfredini T, Romagnoli M. 2004b. The role of sodium hexametaphosphate in the dissolution process of kaolinite and kaolin. *Journal of the European Ceramic Society* 24:2113–2124. DOI: 10.1016/S0955-2219(03)00366-2.

Baars C. 2008. Acid digestion of silicified shells. *Geological Curator* 9:29–33. DOI: 10.55468/GC204.

Bam LC, Miller JA, Becker M, Basson IJ. 2019. X-ray computed tomography: Practical evaluation of beam hardening in iron ore samples. *Minerals Engineering* 131:206–215. DOI: 10.1016/j.mineng.2018.11.010.

Butts SH. 2007. Silicified Carboniferous (Chesterian) Brachiopoda of the Arco Hills Formation, Idaho. *Journal of Paleontology* 81:48–63.

550 Butts SH. 2014. Silicification. *The Paleontological Society Papers* 20:15–34. DOI:
551 10.1017/s1089332600002783.
552 Butts SH, Briggs DEG. 2010. Silicification Through Time. In: 411–434. DOI: 10.1007/978-90-
553 481-8643-3_11.
554 Canfield DE, Raiswell R. 1991. Pyrite Formation and Fossil Preservation. In: 337–387. DOI:
555 10.1007/978-1-4899-5034-5_7.
556 Cherns L, Wheeley J, Wright VP, Allison PA, Bottjer DJ. 2011. Taphonomic bias in shelly faunas
557 through time: Early aragonite dissolution and its implications for the fossil record. In:
558 *Taphonomy, Second Edition: Process and Bias Through Time; Topics in Geobiology 32*.
559 Cooper B, Cooper G. 1946. *DISTRIBUTION OF MIDDLE ORDOVICIAN LIMESTONE*
560 *FORMATIONS IN THE SHENANDOAH VALLEY, VIRGINIA LOWER MIDDLE*
561 *ORDOVICIAN STRATIGRAPHY OF THE SHENANDOAH VALLEY, VIRGINIA*.
562 Dixon P. 2003. VEGAN, a package of R functions for community ecology. *Journal of Vegetation*
563 *Science* 14:927–930. DOI: 10.1111/j.1654-1103.2003.tb02228.x.
564 Donald W. St. Clair. 1935. The Use of Acetic Acid to Obtain Insoluble Residues. *SEPM Journal*
565 *of Sedimentary Research* Vol. 5. DOI: 10.1306/D4268F3B-2B26-11D7-
566 8648000102C1865D.
567 Elkhoury JE, Shankar R, Ramakrishnan TS. 2019. Resolution and Limitations of X-Ray Micro-
568 CT with Applications to Sandstones and Limestones. *Transport in Porous Media* 129:413–
569 425. DOI: 10.1007/s11242-019-01275-1.
570 Evitt WR. 1961. *Early Ontogeny in the Trilobite Family Asaphidae*.
571 Fisher ISJ. 1986. Pyrite replacement of mollusc shells from the Lower Oxford Clay (Jurassic) of
572 England. *Sedimentology* 33:575–585. DOI: 10.1111/j.1365-3091.1986.tb00762.x.
573 Fortey RA, Owens RM. 1999. Feeding habits in trilobites. *Palaeontology* 42:429–465. DOI:
574 10.1111/1475-4983.00080.
575 Grant RE. 1989. Extraction of fossils from carbonates by acid. *The Paleontological Society*
576 *Special Publications* 4:237–243. DOI: 10.1017/S2475262200005190.
577 Green OR. 2001. Extraction Techniques for Phosphatic Fossils. In: *A Manual of Practical*
578 *Laboratory and Field Techniques in Palaeobiology*. Dordrecht: Springer Netherlands, 318–
579 330. DOI: 10.1007/978-94-017-0581-3_27.
580 Hammer Ø, Harper DAT. 2001. PAST: Paleontological Statistics Software Package for
581 Education and Data Analysis. *Palaeontologica Electronica* 4:1–9.
582 Hammer Ø, Harper DAT. 2022. PAST.
583 Holland SM, Patzkowsky ME. 1996. Sequence stratigraphy and long-term paleoceanographic
584 change in the Middle and Upper Ordovician of the eastern United States. In: *Paleozoic*
585 *sequence stratigraphy; views from the North American Craton*. Geological Society of
586 America,. DOI: 10.1130/0-8137-2306-X.117.
587 Jacobs GS, Carlucci JR. 2019. Ontogeny and shape change of the phacopid trilobite
588 Calyptaulax. *Journal of Paleontology* 93:1105–1125. DOI: 10.1017/jpa.2019.38.
589 Jung Y-J, Yun T-S, Kim K-Y, Choo J-H. 2011. Image Calibration Techniques for Removing
590 Cupping and Ring Artifacts in X-ray Micro-CT Images. *Journal of the Korean Geotechnical*
591 *Society* 27:93–101. DOI: 10.7843/kgs.2011.27.11.093.
592 KRAFT JC. 1962. MORPHOLOGIC AND SYSTEMATIC RELATIONSHIPS OF SOME MIDDLE
593 ORDOVICIAN OSTRACODA. In: 1–119. DOI: 10.1130/MEM86-p1.

Kyriakou Y, Prell D, Kalender WA. 2009. Ring artifact correction for high-resolution micro CT. *Physics in Medicine and Biology* 54:N385–N391. DOI: 10.1088/0031-9155/54/17/N02.
Maliva RG, Siever R. 1988. Mechanism and Controls of Silicification of Fossils in Limestones. *The Journal of Geology* 96:387–398. DOI: 10.1086/629235.
Mann HB, Whitney DR. 1947. On a Test of Whether one of Two Random Variables is Stochastically Larger than the Other. *The Annals of Mathematical Statistics* 18:50–60. DOI: 10.1214/aoms/1177730491.
Mitchell CE, Adhya S, Bergström SM, Joy MP, Delano JW. 2004. Discovery of the Ordovician Millbrig K-bentonite Bed in the Trenton Group of New York State: implications for regional correlation and sequence stratigraphy in eastern North America. *Palaeogeography, Palaeoclimatology, Palaeoecology* 210:331–346. DOI: 10.1016/j.palaeo.2004.02.037.
Park HS, Chung YE, Seo JK. 2015. Computed tomographic beam-hardening artefacts: mathematical characterization and analysis. *Philosophical Transactions of the Royal Society A: Mathematical, Physical and Engineering Sciences* 373:20140388. DOI: 10.1098/rsta.2014.0388.
Pruss SB, Payne JL, Westacott S. 2015. Taphonomic bias of selective silicification revealed by paired petrographic and insoluble residue analysis. *Palaios* 30:620–626. DOI: 10.2110/palo.2014.105.
R Core Team. 2021. R: A language and environment for statistical computing.
Read JF. 1980. Carbonate ramp-to-basin transitions and foreland basin evolution, Middle Ordovician, Virginia Appalachians. *The American Association of Petroleum Geologists Bulletin* 64:1575–1612.
Remeysen K, Swennen R. 2006. Beam hardening artifact reduction in microfocus computed tomography for improved quantitative coal characterization. *International Journal of Coal Geology* 67:101–111. DOI: 10.1016/j.coal.2005.10.001.
Roberta L. Daley (*) DWB. 1996. The Role of Skeletal Microstructure During Selective Silicification of Brachiopods. *SEPM Journal of Sedimentary Research* Vol. 66. DOI: 10.1306/D42682E3-2B26-11D7-8648000102C1865D.
Schiffbauer JD, Xiao S, Cai Y, Wallace AF, Hua H, Hunter J, Xu H, Peng Y, Kaufman AJ. 2014. A unifying model for Neoproterozoic–Palaeozoic exceptional fossil preservation through pyritization and carbonaceous compression. *Nature Communications* 5:5754. DOI: 10.1038/ncomms6754.
Schindelin J, Arganda-Carreras I, Frise E, Kaynig V, Longair M, Pietzsch T, Preibisch S, Rueden C, Saalfeld S, Schmid B, Tinevez J-Y, White DJ, Hartenstein V, Eliceiri K, Tomancak P, Cardona A. 2012. Fiji: an open-source platform for biological-image analysis. *Nature Methods* 9:676–682. DOI: 10.1038/nmeth.2019.
Schladitz K. 2011. Quantitative micro-CT. *Journal of Microscopy* 243:111–117. DOI: 10.1111/j.1365-2818.2011.03513.x.
Schubert JK, Kidder DL, Erwin DH. 1997. Silica-replaced fossils through the Phanerozoic. *Geology* 25:1031–1034.
Sell B, Ainsaar L, Leslie S. 2013. Precise timing of the Late Ordovician (Sandbian) super-eruptions and associated environmental, biological, and climatological events. *Journal of the Geological Society* 170:711–714. DOI: 10.1144/jgs2012-148.

637 Wallace AF, DeYoreo JJ, Dove PM. 2009. Kinetics of Silica Nucleation on Carboxyl- and Amine-
638 Terminated Surfaces: Insights for Biomineralization. *Journal of the American Chemical*
639 *Society* 131:5244–5250. DOI: 10.1021/ja809486b.
640 Whittington HB, Evitt WR. 1953. SILICIFIED MIDDLE ORDOVICIAN TRILOBITES. In: 1–169.
641 DOI: 10.1130/MEM59-p1.
642 Yousuf MA, Asaduzzaman M. 2009. An Efficient Ring Artifact Reduction Method Based on
643 Projection Data for Micro-CT Images. *Journal of Scientific Research* 2:37–45. DOI:
644 10.3329/jsr.v2i1.2645.
645
646
647
648

Figure 1

Figure 1

Figure 1. Location map and generalized stratigraphy of samples analyzed in this study. Adapted from Jacobs and Carlucci (2019).

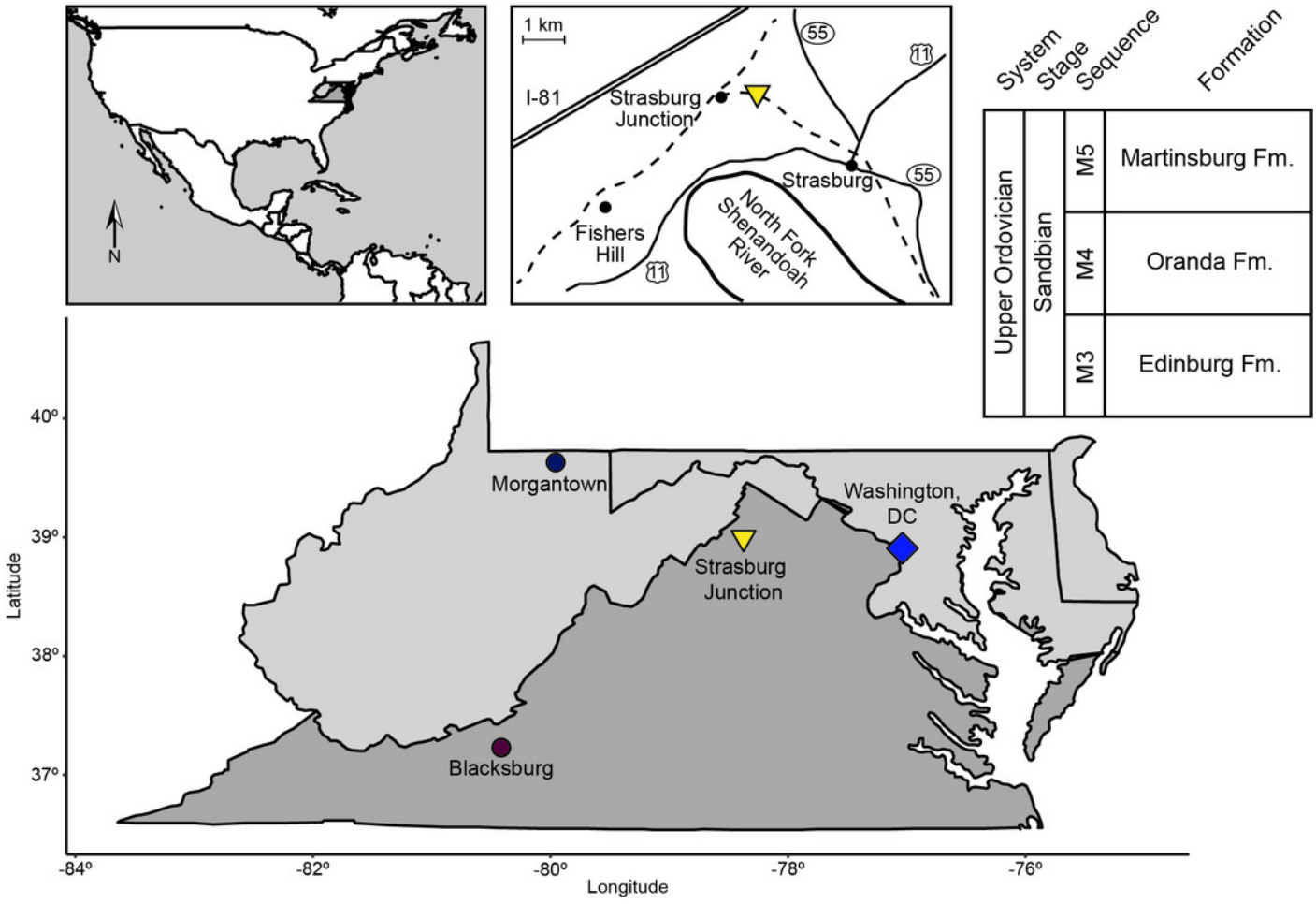

Figure 2

Figure 2

Figure 2. CT renderings of fossils identified in cores of the Edinburg Formation. Blue indicates silica and red indicates Fe-rich mineralization. A) Fenestrate bryozoan (01-C4-001). B) Nuculanid bivalve (03-C3-064) with three small gastropods (03-C3-060, 03-C3-062, 03-C3-065) in pink. C) Closer view of gastropod (03-C3-060). D) Raphiophorid cranidium preserved in silica (05-C4-005) with pyrite infilling (05-C4-047). E) Pterygometopid cephalon (04-C2-028). Note the compound eyes. F) Agnostid fragment (06-C4-027). G) Pterygometopid pygidium (05-C1-019). All scale bars approximate 1 mm.

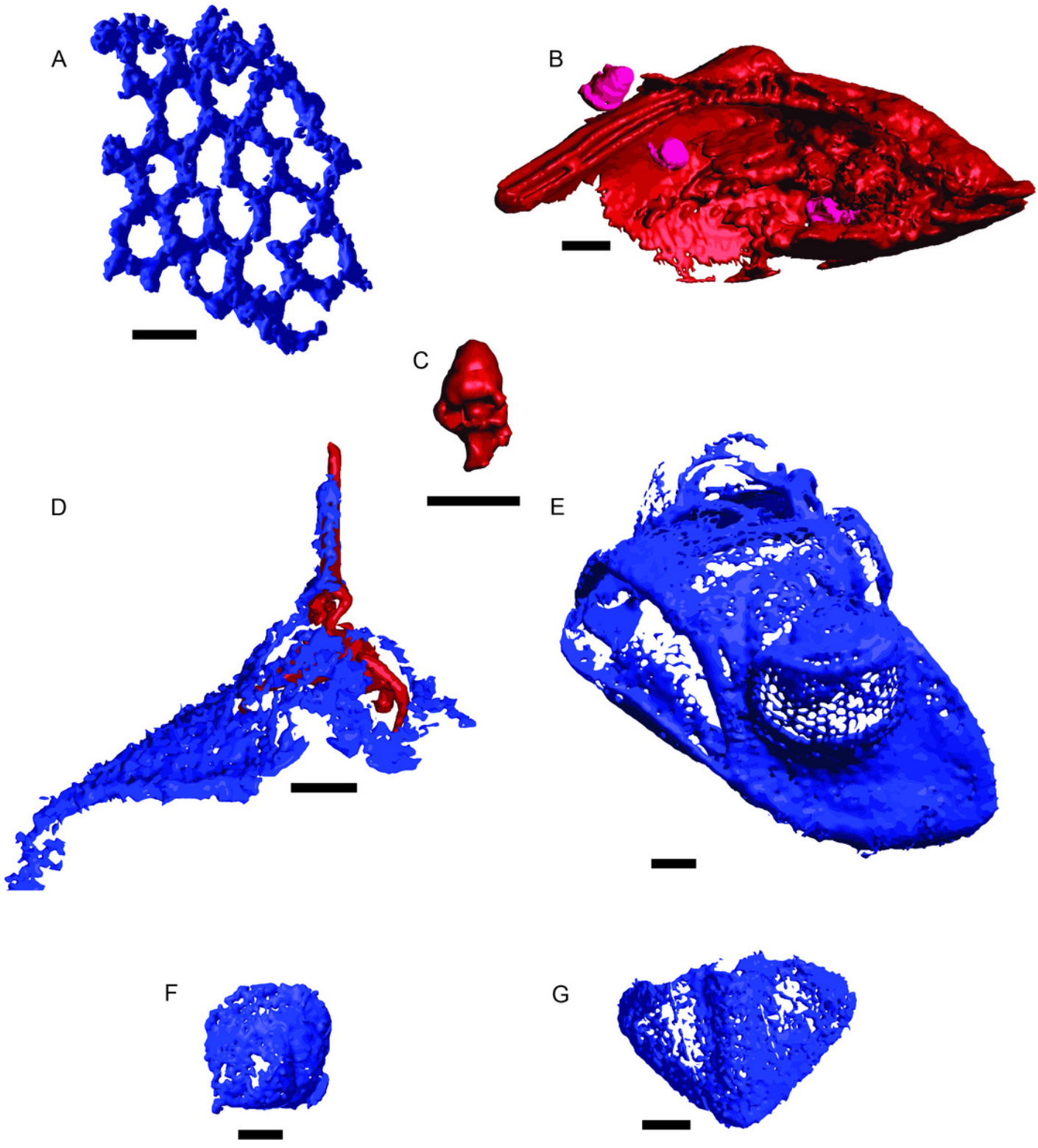
A
B
C
D
E
F
G

Figure 3

Figure 3

Figure 3. Photomicrographs and SEM images of fossils recovered in macerate residues. A) Silicified fenestrate bryozoan (01-C1). B) Silicified erect branching bryozoan (03-C3). C) Pyritized gastropod (03-C3). D) Silicified raphiophorid cranidium (03-C1). E) Silicified *Calyptaulax* cranidium (06-C4). F) Silicified agnostid fragment (06-C4). G) Silicified *Calyptaulax* pygidium (03-C1). H) SEM-image of silicified ostracod valve (04-C1). I) SEM-image of silicified trilobite pygidium (04-C1).

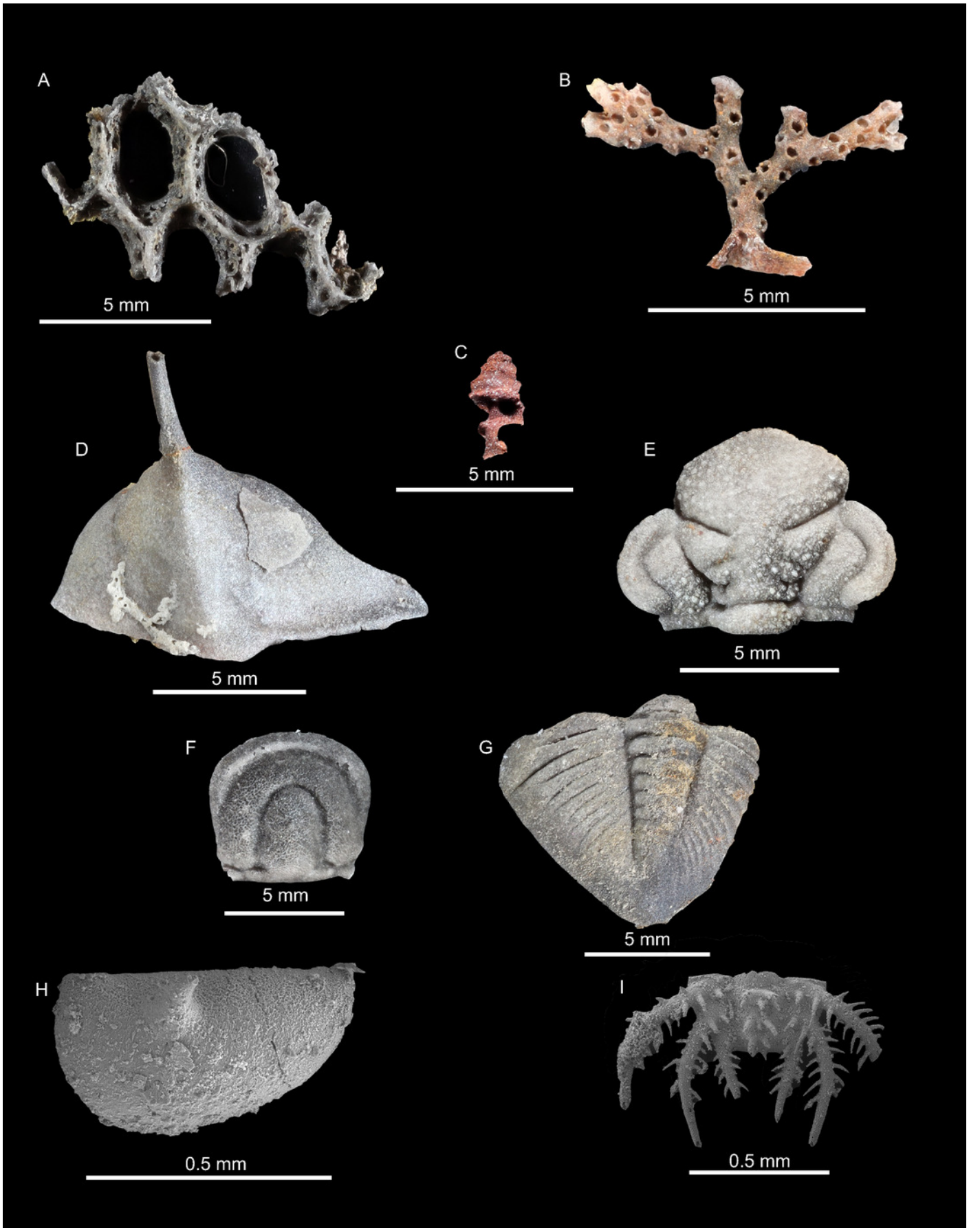
A
5 mm
B
5 mm
C
5 mm
D
5 mm
E
5 mm
F
5 mm
G
5 mm
H
0.5 mm
I
0.5 mm

Figure 4

Fig 4

Figure 4. Results of NMDS of taxon abundance data for A) µCT data (stress = 0.06) and B) acid maceration residue data (stress = 0.08). Samples are plotted as grey squares. Taxon scores are indicated by blue circles. Convex hulls contain samples from each sampling horizon (Table 1). Red: EB18-01. Orange: EB18-03. Yellow: EB18-04. Green: EB18-05. Blue: EB18-06.

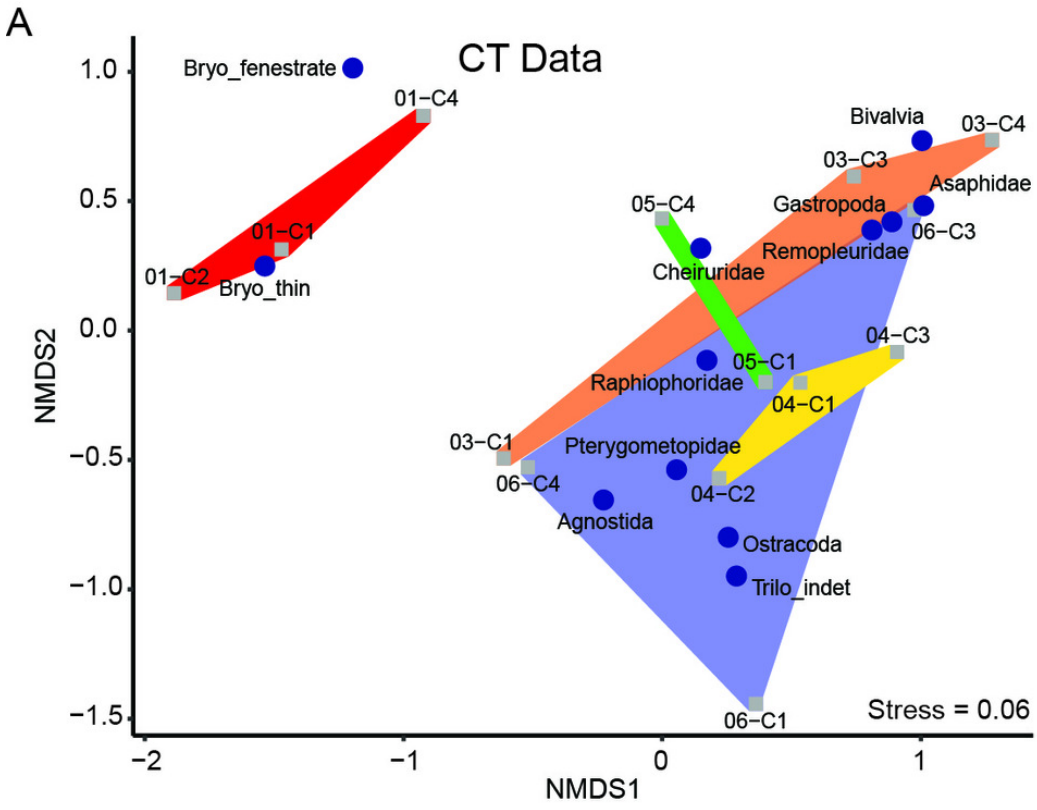
A
CT Data
Bryo_fenestrate
01−C4
01−C1
01−C2
Bryo_thin
Bivalvia
03−C4
03−C3
Asaphidae
05−C4
Gastropoda
06−C3
Remopleuridae
Cheiruridae
04−C3
05−C1
Raphiophoridae
04−C1
03−C1
Pterygometopidae
06−C4
04−C2
Agnostida
Ostracoda
Trilo_indet
06−C1
Stress = 0.06
NMDS1
NMDS2

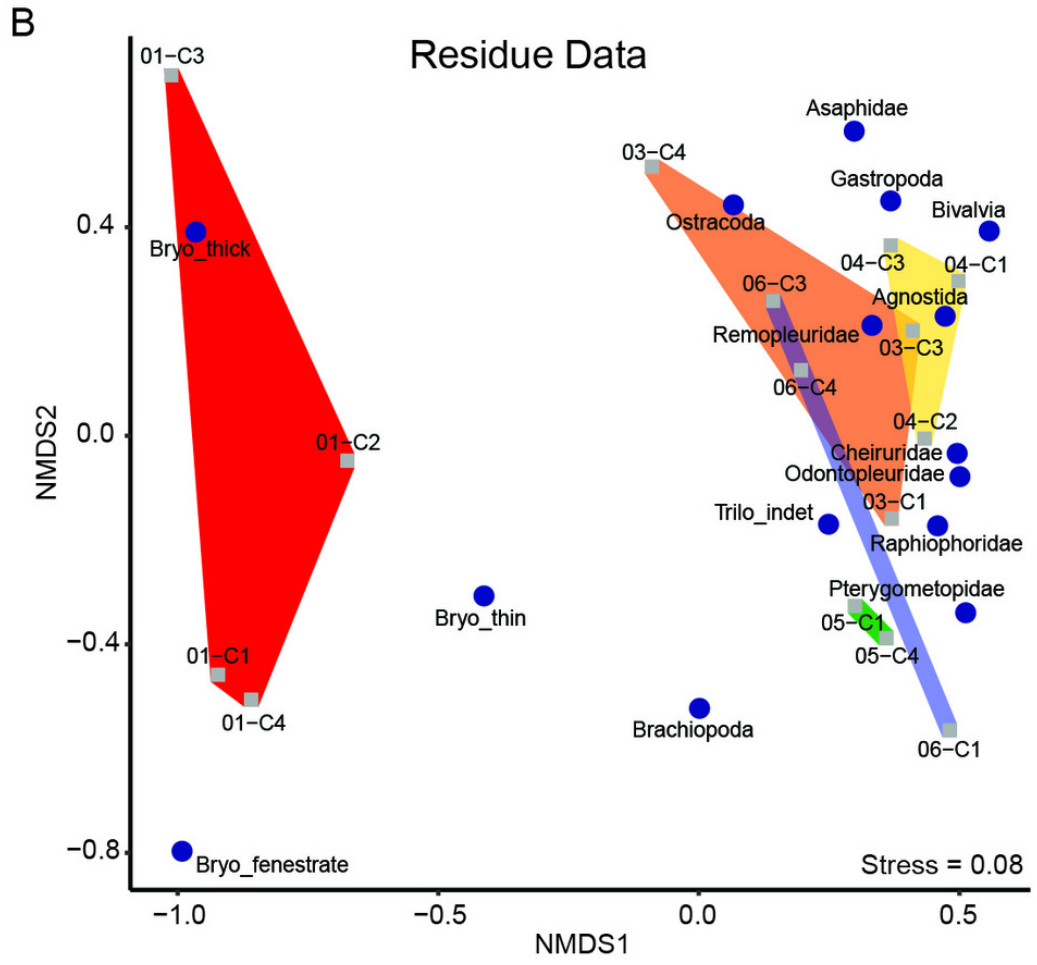
B
Residue Data
01−C3
Asaphidae
03−C4
Gastropoda
Ostracoda
Bivalvia
Bryo_thick
04−C3
04−C1
06−C3
Agnostida
Remopleuridae
03−C3
06−C4
04−C2
01−C2
Cheiruridae
Odontopleuridae
03−C1
Trilo_indet
Raphiophoridae
Pterygometopidae
Bryo_thin
05−C1
05−C4
01−C1
Brachiopoda
01−C4
06−C1
Bryo_fenestrate
Stress = 0.08
NMDS1
NMDS2

Figure 5

Fig 5

Figure 5. Simpson's Dominance (D) and bootstrapped 95% confidence intervals calculated for each sample by data type. data are in blue and acid maceration residue data are in orange.

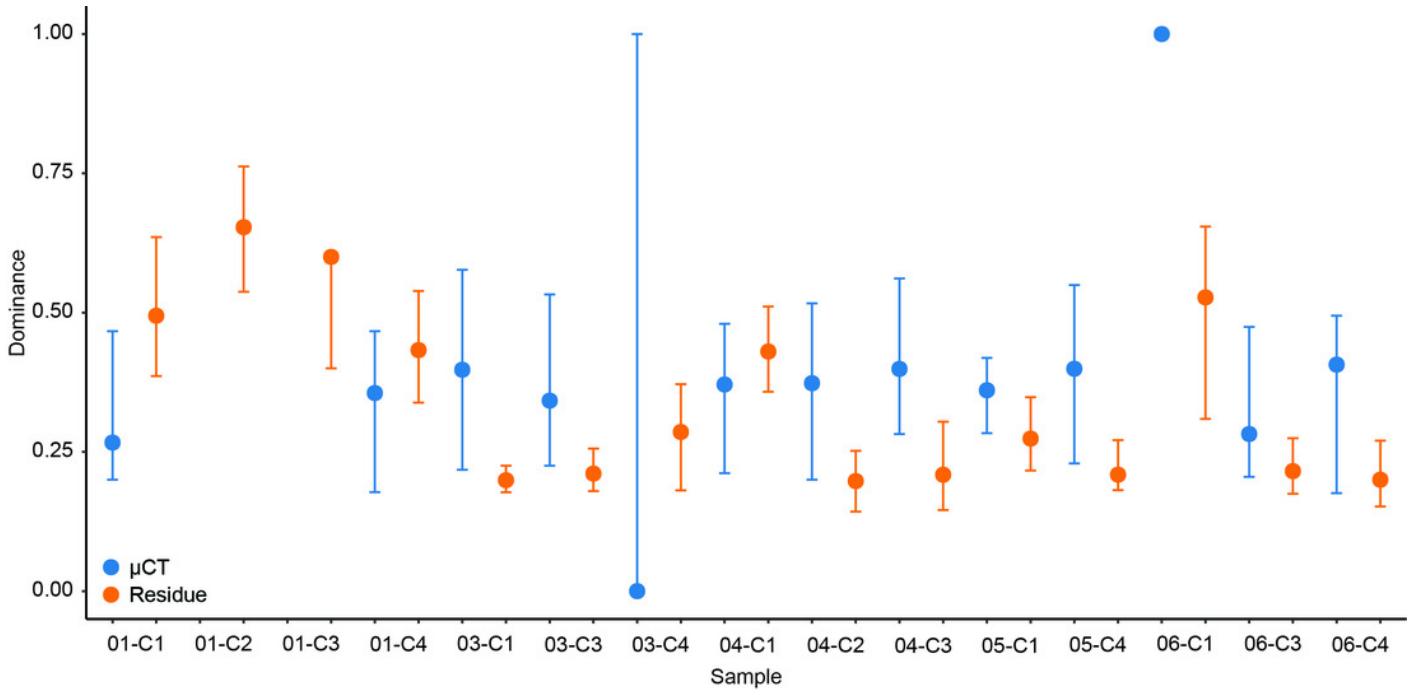

Figure 6

Fig 6

Figure 6. Rarefaction analysis of taxonomic richness for A) µCT samples (Table 6) and B) acid maceration residue samples (Table 7).

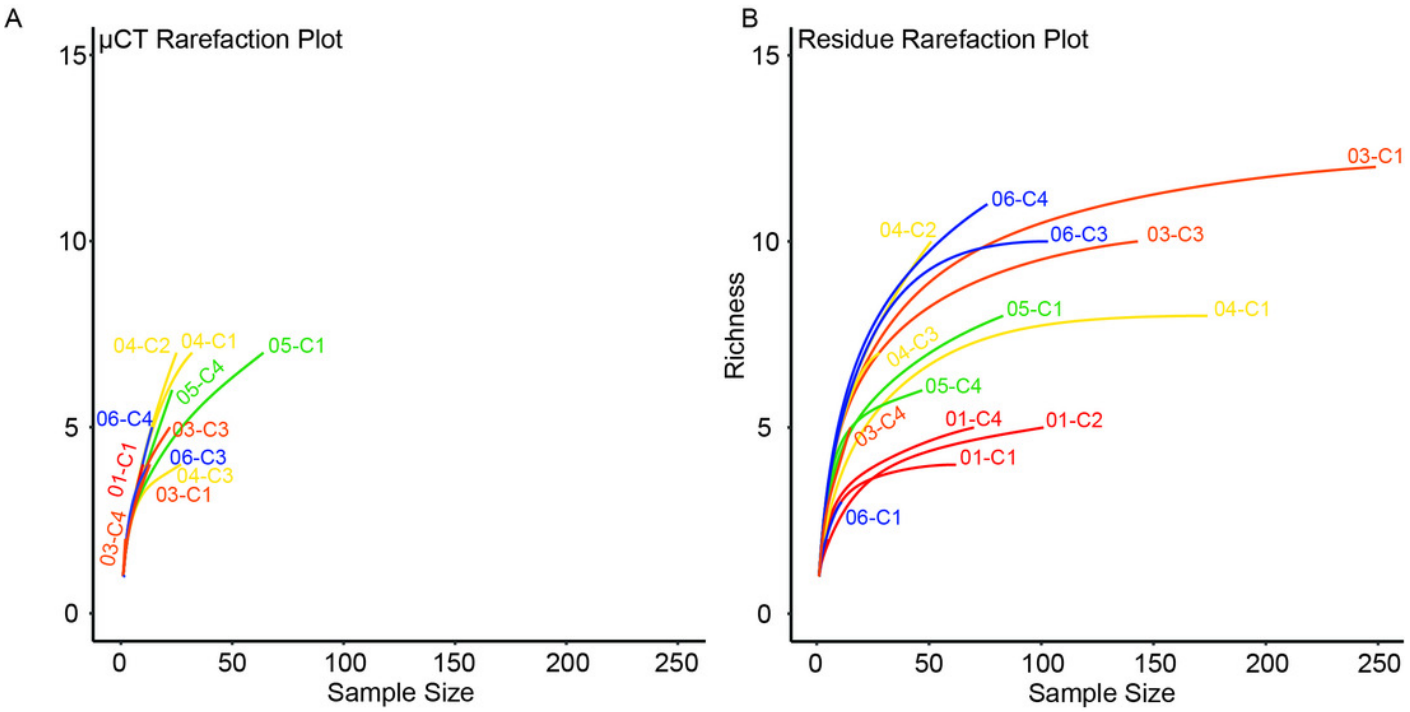

Figure 7

Fig 7

Figure 7. Bray-Curtis similarity dendrograms of taxon abundance values in A) µCT samples (Table 6) and B) acid maceration residue samples (Table 7) calculated separately.

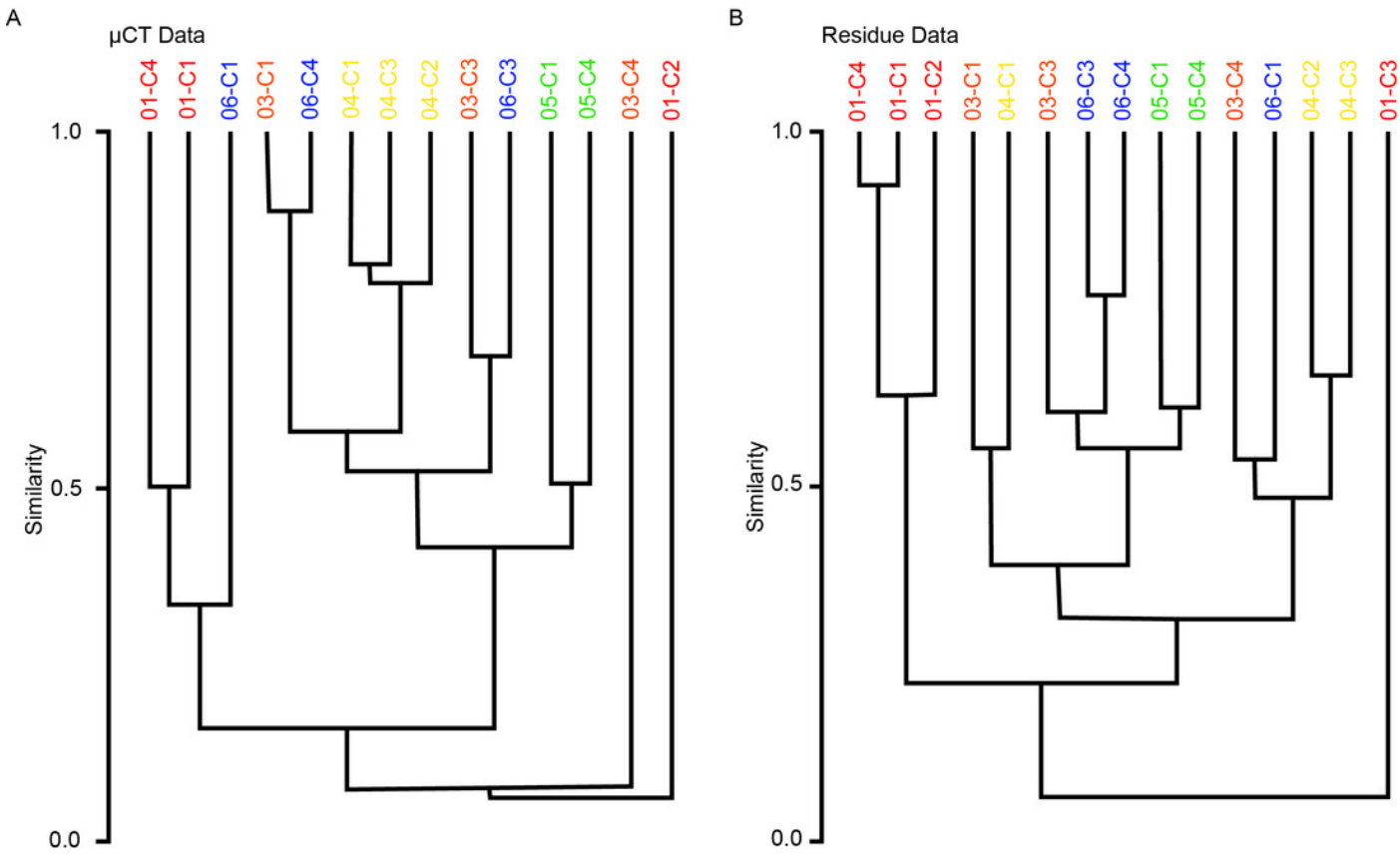

Figure 8

Fig 8

Figure 8. Bray-Curtis similarity dendrograms of pooled taxon abundance values in µCT samples (Table 6) and acid maceration residue samples (Table 7).

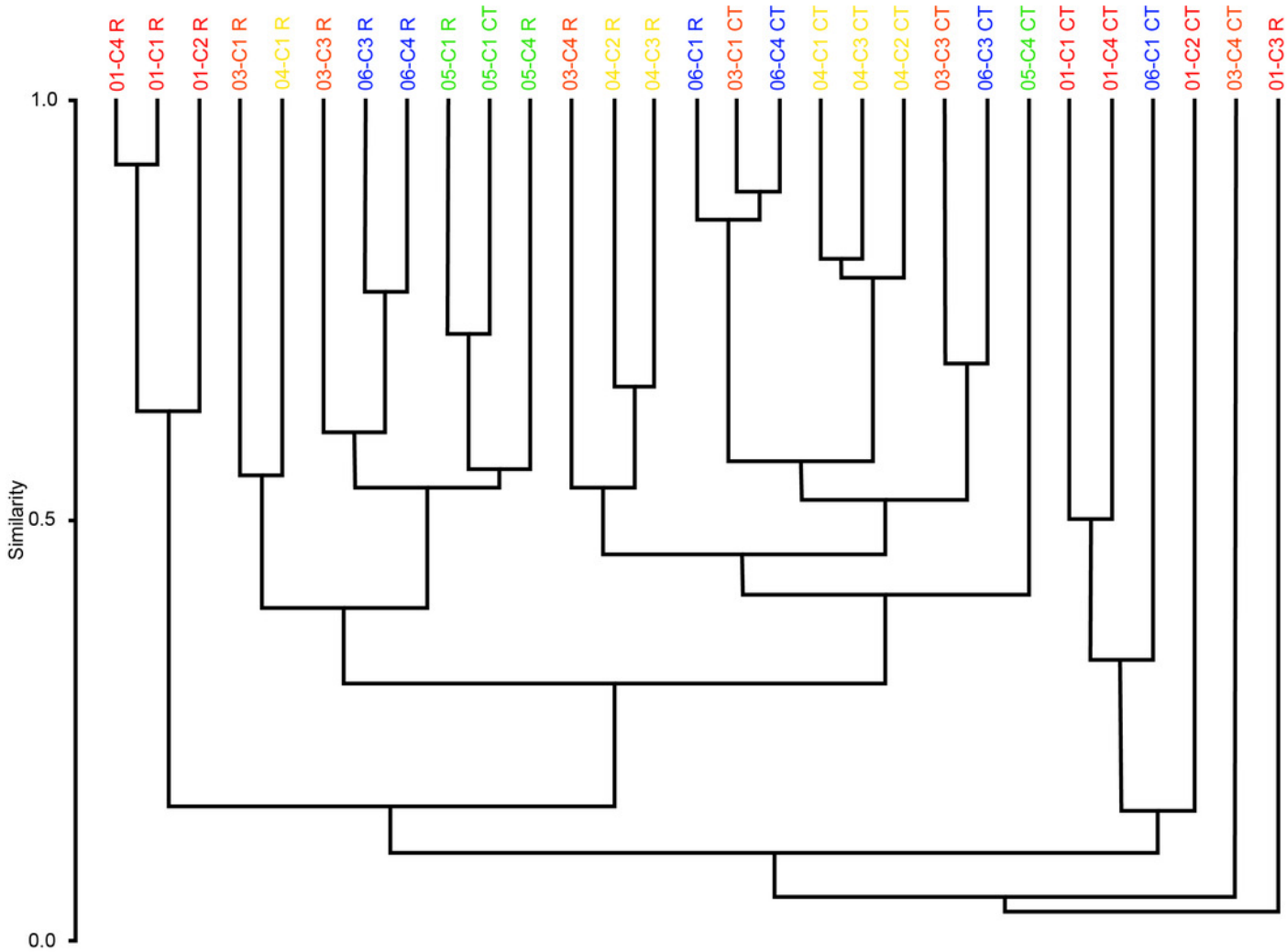

Table 1(on next page)

Tables 1-8

This file contains all eight tables each with the appropriate legend

Tables

Horizon	Latitude	Longitude	Notes
EB18-01	38.9969°N	78.3748°W	~0.5 m above contact between Lincolnshire LS and Edinburg Fm
EB18-03	38.9968°N	78.3744°W	~20-30 m up section from EB18-01
EB18-04	—	—	0.5 m up section from EB18-03
EB18-05	—	—	1.0 m up section from EB18-04
EB18-06	—	—	~5 m up section from EB18-05

Table 1. Summary of horizons and samples used in this study.

Taxon		Measurements and Classifications
Trilobita	Cranidium	Maximum width (tr.) of occipital lobe*, maximum width (tr.) between eyes**, total length (sag.)
	Thoracic segment	Maximum width (tr.) of axial ring, width (tr.) between fulcra of left and right pleurae, length (sag.) of axial ring
	Pygidium	Maximum width (tr.) of first axial ring, total length (sag.)
Bryozoa		Growth form: dendroid or fenestrate
Gastropoda		Presence/absence of outer walls of whorls, total height of shell, height of last complete whorl, width of last complete whorl, half-angle of teleoconch***
Ostracoda		Body length (a.-p.), body height (d.-v.), articulation/disarticulation, presence/absence of lateral spine

Table 2. Anatomical measurements and classifications by taxon and sclerite. Measurements taken from CT and residue imagery for each of several common taxa. The main sclerites of trilobites (excluding hypostomes and librigenae) were assigned different sets of measurements due to fundamental differences in structure. Lengths, widths, and heights are measured in mm; angles are measured in degrees; other category variables were recorded as Booleans.
* Raphiophorids have an effaced prosopon with indistinct furrows, making identification of the occipital lobe difficult in CT especially. For this family of trilobites, occipital width was instead measured as the full width (tr.) of the sclerite from gena to gena at the occiput.
** For eyeless trilobites of the families Metagnostidae and Raphiophoridae, interocular distance was excluded.
*** This is the angle formed at the apex between the axis of coiling and a line tangent to the outer walls of the body whorls.

Taxon		µCT	Residues
Total Trilobita		225	594
Trilobita	Asaphidae	6	20
	Cheiruridae	2	3
	Metagnostidae	6	14
	Odontopleuridae	0	18
	Pterygometopidae	6	41
	Raphiophoridae	57	149
	Remopleurididae	22	59
	Unknown Trilobita	126	290
Bivalvia		2	1
Brachiopoda		0	5
Bryozoa	Thin branching	9	304
	Thick branching	0	49
	Fenestrate	7	22
Gastropoda		10	11
Ostracoda		1	232
Unknown		327	161
Total		**581**	**1379**

Table 3. Fossils Recovered by Preparation Method and Taxon. Total counts of all objects identified in CT and residue imagery, grouped by taxon. Trilobites are further broken down to the family level. Trilobite material lacking sufficient anatomical features to be confidently assigned to a family was given its own category.

Taxon	Not Recovered	Recovered	Recovered residual	p-value
Asaphidae	3	2	0.213	0.84
Cheiruridae	1	1	0.285	0.67
Metagnostidae	2	4	1.855	0.11
Pterygometopidae	4	1	-0.787	0.46
Raphiophoridae	37	20	-0.376	0.90
Remopleurididae	13	8	0.493	0.81
Unknown Trilobita	71	28	-7.389	0.04
Bivalvia	1	1	0.285	0.67
Bryozoa (thin)	4	4	1.140	0.39
Bryozoa (fenestrate)	2	4	1.855	0.11
Gastropoda	4	6	2.425	0.10

Table 4. Taxonomic Effects on Recovery. Contingency table containing counts of fossils with distinctive geometry identified in CT imagery and either recovered or not recovered in residue. Residuals of recovered counts are standardized to the expected number of recovered specimens for a taxon; positive residuals indicate disproportionately high likelihood of recovery in residues, while negative values indicate lower-than-average likelihood of recovery. Statistically significant results ($p < 0.05$) are shaded.

Taxon	CT	Residue	CT residual	Residue residual	p-value
Asaphidae	6	20	0.715	-0.326	0.43
Cheiruridae	2	3	1.224	-0.559	0.18
Metagnostidae	6	14	1.372	-0.627	0.13
Odontopleuridae	0	18	-1.762	0.805	0.05
Pterygometopidae	6	41	-0.741	0.338	0.41
Raphiophoridae	57	149	3.598	-1.643	2.0 E-05
Remopleurididae	22	59	2.146	-0.980	0.02
Unknown Trilobita	126	290	6.399	-2.922	9.9 E-17
Bivalvia	2	1	2.060	-0.941	0.02
Brachiopoda	0	5	-0.929	0.424	0.31
Bryozoa (thin)	9	304	-6.125	2.797	3.3 E-14
Bryozoa (thick)	0	49	-2.908	1.328	1.2 E-3
Bryozoa (fenestrate)	7	22	0.892	-0.407	0.32
Gastropoda	10	11	3.350	-1.530	2.1 E-4
Ostracoda	1	232	-6.183	2.824	1.3 E-13

Table 5. Comparison of Taxonomic Abundances. Contingency table containing total counts of taxa identified in CT and in residue imagery. Residuals of recovered counts are standardized to the expected number of recovered specimens for the combination of taxon and preparation; positive CT residuals indicate overrepresentation in CT for that taxon, while positive residue residuals indicate overrepresentation in residues (relative to average proportional abundance for all fossils). Statistically significant results ($p < 0.05$) are shaded.

	01-C1	01-C2	01-C4	03-C1	03-C3	03-C4	04-C1	04-C2	04-C3	05-C1	05-C4	06-C1	06-C3	06-C4	**Sum**
Agnostida	0	0	0	1	0	0	1	2	0	1	0	0	0	1	**6**
Asaphidae	0	0	0	0	0	1	2	0	1	1	1	0	0	0	**6**
Cheiruridae	0	0	0	0	0	0	0	0	0	1	1	0	0	0	**2**
Odontopleuridae	0	0	0	0	0	0	0	0	0	0	0	0	0	0	**0**
Pterygometopidae	0	0	0	0	0	0	1	1	0	3	0	0	0	1	**6**
Raphiophoridae	0	0	0	3	1	0	5	4	5	23	14	0	0	2	**57**
Remopleuridae	0	0	1	0	5	1	2	1	5	4	1	0	2	0	**22**
Trilo indet	2	0	1	8	12	0	19	15	16	31	5	2	6	9	**126**
Bivalvia	0	0	0	0	1	0	0	0	0	0	0	0	1	0	**2**
Brachiopoda	0	0	0	0	0	0	0	0	0	0	0	0	0	0	**0**
Bryo thin	3	1	2	1	0	0	0	0	0	0	1	0	0	1	**9**
Bryo thick	0	0	0	0	0	0	0	0	0	0	0	0	0	0	**0**
Bryo fenestrate	1	0	6	0	0	0	0	0	0	0	0	0	0	0	**7**
Gastropoda	0	0	0	0	3	0	2	1	0	0	0	0	4	0	**10**
Ostracoda	0	0	0	0	0	0	0	1	0	0	0	0	0	0	**1**
SUM	**6**	**1**	**10**	**13**	**22**	**2**	**32**	**25**	**27**	**64**	**23**	**2**	**13**	**14**	

Table 6. Abundance of taxonomic groups identified in CT data used in NMDS.

62

	01-C1	01-C2	01-C3	01-C4	03-C1	03-C3	03-C4	04-C1	04-C2	04-C3	05-C1	05-C4	06-C1	06-C3	06-C4	**Sum**
Agnostida	0	0	0	0	6	2	0	2	1	0	0	0	0	2	1	**14**
Asaphidae	0	0	0	0	0	2	1	4	1	2	0	0	0	4	6	**20**
Cheiruridae	0	0	0	0	1	0	0	0	0	1	0	1	0	0	0	**3**
Odontopleuridae	0	0	0	0	9	0	0	4	1	0	3	0	0	0	1	**18**
Pterygometopidae	0	0	0	0	12	4	0	5	2	0	1	5	1	4	7	**41**
Raphiophoridae	0	0	0	0	59	8	1	21	7	2	19	12	2	10	8	**149**
Remopleuridae	0	1	0	0	8	30	0	6	2	2	2	0	0	4	4	**59**
Trilo indet	2	8	0	2	72	51	6	22	17	8	37	12	8	29	16	**290**
Bivalvia	0	0	0	0	0	1	0	0	0	0	0	0	0	0	0	**1**
Brachiopoda	0	0	0	1	2	0	0	0	1	0	1	0	0	0	0	**5**
Bryo thin	42	81	0	43	17	24	0	0	6	3	11	13	0	36	28	**304**
Bryo thick	8	8	4	15	4	0	1	0	0	0	0	0	0	7	2	**49**
Bryo fenestrate	10	0	0	9	2	0	0	0	0	0	0	0	0	0	1	**22**
Gastropoda	0	0	0	0	0	6	0	0	0	0	0	0	0	5	0	**11**
Ostracoda	0	3	1	0	57	15	6	110	13	10	9	4	0	2	2	**232**
SUM	**62**	**101**	**5**	**70**	**249**	**143**	**15**	**174**	**51**	**28**	**83**	**47**	**11**	**103**	**76**	

63

64 Table 7. Abundance of taxonomic groups recovered in acid maceration residues used in NMDS.

65